Article

A Numerical Study on the Characteristics of the Pressurized Water Reactor's (PWR) Primary Moisture Separator Using the Particle Tracking Method

Hongwu Zhao [1], Jun-Ho Jeon [2], Dong-In Yu [3] and Yeon-Won Lee [3,*]

1   Department of Mechanical Design Engineering, Graduate School of Pukyong National University,
     Busan 48513, Republic of Korea
2   PIBEX Inc., CAE Team, Pohang 37668, Republic of Korea
3   School of Mechanical Engineering, Pukyong National University, Busan 48513, Republic of Korea
*   Correspondence: ywlee@pknu.ac.kr; Tel.: +82-51-629-6162

Abstract: The primary moisture separator—a key component in the PWR nuclear power plant—determines the quality of supplied steam to a turbine. Investigating its characteristics is important because supplying steam with excessive droplet entrainment results in damages to pipes, valves, and turbines in power plant circuits. In this numerical study, the particle tracking method in the Eulerian–Lagrangian methodology is used to investigate the characteristics of a primary moisture separator. Various swirl vanes with different bending angles, vane quantities, and vane locations are chosen to investigate the effect of design parameters on characteristics of the primary moisture separator. Additionally, the water droplet size is considered to vary from 0.01 to 50 μm in this study. The pressure drop between the inlet and outlet, the steam quality at the orifice outlet, and the particle collection ratio are discussed in this paper. The results show that steam quality increases as the bending angle decreases, and increasing the number of swirl vanes increases both the pressure drop and the steam quality.

Keywords: primary moisture separator; swirl vane; droplet size; particle tracking method; CFD

1. Introduction

Nuclear power plants, when compared with coal-fired power plants, do not emit carbon dioxide, sulfur dioxide, nitrogen oxides, and other environmentally damaging emissions. They can be considered as one of the alternatives to traditional fossil fuel power plants in terms of environmental protection. There has been little growth in fossil fuel power plants in the past ten years. On the contrary, the development of nuclear power is gaining importance all over the world [1]. Therefore, research on nuclear power has become a popular research project in many countries. In this study, the PWR's primary moisture separator is the target of this investigation. The primary moisture separator, located in the upper part of the steam generator, plays a key role in the system [2]. The mixture flow into the moisture separator becomes the swirl flow after the swirl vane. The swirl flow is generated by a swirling motion that imparts a swirl velocity component to the flow, by using an axial-plus-tangent entry into the vortex generator, or by tangential entry into the chamber [3]. This swirl flow makes the droplets migrate towards the wall of the riser and forms a thin water film on the wall. Due to the density differences between the water droplet and the vapor, the water droplets are separated from the mixture. More than 80% of the droplets generated in the steam generator should be separated by the primary moisture separator [4].

Numerous researchers have studied the characteristics of the primary moisture separator. Several scholars have focused on the theoretical study of the separator. Qu et al. [5],

Najafi et al. [6], and Saqr et al. [7] mainly investigated the importance of the swirl intensity in the process of separating. Liu et al. [8] developed a mechanistic model for the prediction of swirling annular flow pattern transitions. Based on their investigation, they concluded that the annular flow property was related to the critical film thickness and critical gas/liquid velocity. These scholars' results illustrated that the newly developed correlation yielded a more accurate transition flow pattern prediction for swirl flows. Additionally, Liu et al. [9] mathematically investigated separators and proposed a scaling law that enabled a comparison between the reduced and full-scale model. Based on the scaling theory, several scholars investigated the separator through the experimental method. Matsubayashi et al. [10], Kataoka et al. [4], and Funahashi et al. [11,12] studied the boiling water reactor's (BWR) separator by changing the geometry, including the bending angle and the vane quantity, and by adding pick-off rings. The pressure drop or separation was related to these parameter designs. Furthermore, Nishida et al. [13] developed a new design with a swirl vane hub with a small diameter and horizontal slits at the riser barrel. This design could also strongly prevent vane damage. Nevertheless, Xiong et al. [14], Kataoka et al. [15], and Funahashi et al. [16] experimentally investigated the separator by changing the mixture velocity or single phase flux. Their experimental studies were mostly focused on the geometry design or the changing inlet conditions.

In comparison to the experimental approach, which always needs to consider the scaling law, the numerical approach can easily overcome this scaling problem. Due to the development of computer technology in the past few decades, the numerical analysis has sufficient robustness for determining the characteristics of the moisture separator, as long as the appropriate model is selected [17]. Tamrina et al. [18] concluded that the higher-order discretization scheme yielded a better result compared to the first-order scheme. Zhang et al. [19,20] numerically studied both primary and secondary separators of the AP1000 geometry. Their results illustrated the primary stage separation efficiency with different inlet humidity values. Tian et al. [21] numerical studied a new structure of separators. They concluded that reducing the cylinder diameter could increase the separation effect. Kataoka et al. [22] used numerical methods to investigate the pressure drop and film thickness in a moisture separator. After changing the gas and liquid volume fluxes, the results illustrated that the pressure drop with a swirling flow was about five times that with a nonswirling flow. Huang et al. [20] and Song et al. [23] numerically studied the separation process of the moisture separator. They verified the feasibility of the numerical analysis and concluded that the data matched the experiment. Fang et al. [2,24] studied a full-scale numerical model regarding the process from the moisture separator to the dryer and then compared the difference between the moisture separator and the dryer. Their conclusions showed that the separator simulation should consider the cold leg and hot leg in the steam generator. Saito et al. [25] numerically analyzed the droplet behavior of the BWR's moisture separator. They concluded that the deposition coefficient would increase by adding the swirl intensity. Katono et al. [26] numerically and experimentally studied the down-scale moisture separator characteristics by moving the swirl vane section. The results showed that a modified separator could reduce the pressure drop by more than 50%. Xiong et al. [27] developed an experiment and simulation on a 1:3.5 scale swirl vane separator and investigated both the separation efficiency and pressure drop. The conclusions illustrated that the pressure was mainly affected by the airflow rate and water droplet size. Rocha et al. [28] developed an axially induced swirling pipe flow through numerical and experimental studies. They concluded that smaller gap widths and larger deflection angles could provide more swirls. This result can be beneficial for applications that require swirling over a longer pipeline distance.

Based on the above literature review, we found that most numerical investigations on moisture separators used the volume of fluid (VOF) method. However, we know that the approach to dealing with numerically capturing interfaces is an established field in CFD communities [29]. Logically, this kind of multiphase flow problem can be classified as a continuity phase and a dispersed phase, which are solved through Eulerian and

Lagrangian approaches, respectively [30,31]. Zhang et al. [19,21,27] used the VOF method. However, the particle tracking multiphase model mentioned in Fang et al. [29,32,33] was used for a bubble flow. The target in this study focused on capturing droplet particles in moisture separators. Judging from the property of moisture flow, the droplets are transported by the steam. In order to classify the process of capturing particles during the moisture flow through the moisture separator, a suitable approach should be considered. The particle tracking method is suitable for this study, even though it is simple. The particle tracking model based on the Lagrangian–Eulerian methodology is used here to study the characteristics of the primary moisture separator. Since the droplet particles follow the steam flow during the flow process, the effect of the droplet particles on the steam flow is ignored, and a one-way coupling is applied in the simulation process.

Although previous researchers have made many research contributions in this field, the research on moisture separators is still insufficient. Here, we focus on the moisture separator's droplet-capturing process by using the particle tracking method. In addition, we investigate the effects of different moisture separator models aiming to increase the separator's outlet steam quality and decrease the pressure drop. We also aim to improve the separation efficiency of the moisture separators. This study can act as a relevant reference for future designs and research. In this numerical study, the particle tracking method in the Eulerian–Lagrangian methodology is used to investigate the characteristics of the primary moisture separator. Different swirl vane bending angles, different quantities of swirl vanes, and different swirl vane locations are chosen to investigate the characteristics of the primary moisture separator. Moreover, various water droplet sizes—from 0.01 to 50 μm—are also considered in this study.

2. Numerical Analysis

The moisture separator model comes from the general model of the steam generator of the pressurized water reactor in a nuclear power plant [34]. Figure 1 shows the schematic of the computational domain used and the mesh generation in this study. It includes a tangent nozzle outlet, an orifice outlet, a downcomer outlet, a riser, swirl vanes, and an inlet.
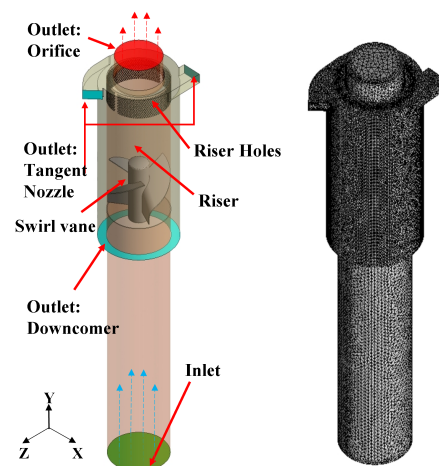

Figure 1. Schematic of the computational domain and the mesh generation.

2.1. Governing Equations

2.1.1. Continuous and Dispersed Fluid

The process of moisture flow in the separator was considered adiabatic so that we only needed to calculate the continuity and momentum equation. The moisture flow was

classified into a continuous fluid-steam and dispersed fluid–water particle. The governing equations that describe the flow of the continuous fluid are given below [30,35,36].

$$\frac{\partial \rho}{\partial t} + \frac{\partial \rho u_i}{\partial x_i} = 0 \tag{1}$$

$$\frac{\partial(\rho u_i)}{\partial t} + \frac{\partial(\rho u_i u_j)}{\partial x_j} = -\frac{\partial p}{\partial x_i} + \frac{\partial}{\partial x_j}[\mu(\frac{\partial u_i}{\partial x_j} + \frac{\partial u_j}{\partial x_i})] + S_M \tag{2}$$

where ρ, u, p, μ, and S_M are the density, velocity, pressure, viscosity, and the sum of body force, respectively. For turbulence models, the $k - \epsilon$ model, the baseline (BSL) $k - \omega$ model, and the shear stress transport (SST) $k - \omega$ model were compared. The simulation results showed that the BSL model was not suitable for the particle tracking model when compared to the results of the $k - \epsilon$ model and the SST $k - \omega$ model. Previous researchers compared the model simulations, and the results showed that the SST $k - \omega$ model had stronger adaptability to the swirl flow compared to the $k - \epsilon$ model [17,21]. The BSL model failed to predict the onset and the amount of flow separation from the smooth surfaces, despite combining the Wilcox and the $k - \epsilon$ model. This is why these models do not account for the transport of the turbulent shear stress and overpredict the eddy viscosity [30]. For these reasons, the SST $k - \omega$ model was applied in this study. The SST $k - \omega$ model solves the two transport equations, namely, one for the turbulent kinetic energy and the other for the turbulent frequency. The stress tensor is computed from the eddy viscosity equation [30]. The SST $k - \omega$ model assumes that the turbulence viscosity is linked to the turbulence kinetic energy k and the turbulent frequency ω through the equations.

$$\mu_t = \rho \frac{k}{\omega} \tag{3}$$

$$\frac{\partial(\rho k)}{\partial t} + \frac{\partial}{\partial x_j}(\rho u_j k) = \frac{\partial}{\partial x_j}[(\mu + \frac{\mu_t}{\sigma_k})\frac{\partial k}{\partial x_j}] + P_k - \beta' \rho k \omega + P_{kb} \tag{4}$$

$$\frac{\partial(\rho \omega)}{\partial t} + \frac{\partial}{\partial x_j}(\rho u_j \omega) = \frac{\partial}{\partial x_j}[(\mu + \frac{\mu_t}{\sigma_\omega})\frac{\partial \omega}{\partial x_j}] + \alpha \frac{\omega}{k} P_k - \beta \rho \omega^2 + P_{\omega b} \tag{5}$$

where μ_t, k, and ω are the turbulence viscosity, kinetic energy, and turbulence frequency, respectively. σ, β, and P are the constant coefficients for the turbulence model. Their specific expression can be found in [30].

2.1.2. Particle Tracking Methodology

In the process of Lagrange particle implementation, a specified portion of particles represents all of the particles in the flow through the continuum fluid during particle transport. The discrete particle moves in the continuous fluid medium. Such a particle's motion is driven by the force exchange between the continuum and discrete media. The process equations are derived from Basset, Boussinesq, and Oseen [30]. The equations are as follows:

$$\frac{dx_p}{dt} = U_p \tag{6}$$

$$x_p^n = x_p^o + U_p^o \delta_t \tag{7}$$

$$m_p \frac{dU_p}{dt} = F_D + F_B + F_R + F_{vm} + F_P + F_{BA} \tag{8}$$

$$m_p = \frac{\pi}{6} d_p^3 \rho_p \tag{9}$$

where x_p, U_p^o, and m_p are the particle displacement, the initial particle velocity, and the mass of the particle, respectively. The superscripts o and n refer to old and new values, respec-

tively. These equations describe the method to calculate the particle variables and the realization of the interphase transfer through the particle transport model. Equations (6) and (7) illustrate the calculation of the new value of one particle during the simulation, and δ_t represents the timestep. The variables F_D, F_B, F_R, F_{VM}, F_P, and F_{BA} in Equation (8), respectively, represent the drag force acting on the particle, the buoyancy force due to gravity, the forces due to domain rotation, the virtual mass force, the pressure gradient force, and the Basset force or history term that accounts for the deviation in flow pattern from a steady state.

2.2. Modeling and Analysis

The mixture in the moisture separator is swirled by a swirl vane in the moisture separator. Due to the differences in density, the droplet particles with a larger mass are subjected to more centrifugal force, leading to a move towards the riser wall. Several droplets in the mixture are captured and separated by the riser wall and become the reflux of the downcomer. Some of the droplets come out of the separator's tangent nozzle into the steam generator's gravity space. The particles are returned to the steam generator for further separating due to the action of gravity.

According to the automatic near-wall treatment method requirements of the CFX [30], the first node distance should avoid the buffer layer. The solver will choose a suitable treatment based on the detection Y-plus value. For this study case, a Y-plus value between 30 and 200 was chosen, which means the Y-plus was located at the log-law layer of the boundary layer. This solution approach used a fully implicit discretization of the equations at any given time scales—set as 0.04 s. Since the particle tracking method selected a certain number of particles to substitute for all the droplet particles in the simulation [30], a particle-quantity-sensitive study became necessary. The particle numbers were chosen from 100 to 20,000, which were distributed randomly in the geometry inlet to inspect the influence of the particle numbers. When the number of particles exceeded 1000, the result of the steam quality at the orifice outlet tended to be constant. Nevertheless, in order to test sufficient particles, the number of particles in different cases was chosen as 10,000 to represent all the water particles in this study.

When the particles collide with each other and with the separator wall, we considered the exchange momentum only with the wall. During such collisions, the momentum loss is controlled by constant or time-dependent coefficients of restitution. In the case of a fully inelastic collision, the particles are collected on the wall. Generally, the droplets will migrate to the wall and become a film after contact with the separator surface. The model enforced that all particles hitting the wall became part of the wall film, regardless of their impact velocity or impact angle. To terminate the tracking of particles when they hit a wall boundary, both the perpendicular and parallel coefficients could be set to zero. The particle then came to a stop regardless of what was set for the parallel coefficient of restitution.

Figure 2 shows the schematic of the wall treatment method described above. When the parallel and perpendicular restitution coefficient is set to 1, the particle fully rebounds, and when both the coefficients are set to 0, the particles do not rebound because they are captured by the wall when they are in contact. The restitution coefficient was set to 0 in this study.
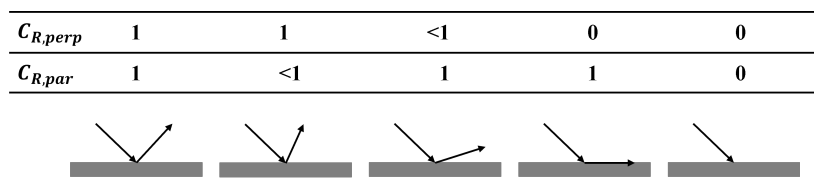
$C_{R,perp}$	1	1	<1	0	0
$C_{R,par}$	1	<1	1	1	0

Figure 2. The schematic of the wall treatment method [30].

Since the separator consists of many curved surfaces and small holes, the tetra/mixed type meshing was used to better fit the mesh with the model. For the partitioning methods, the robust mode by which sufficient parts are divided was used. To accurately capture the

boundary layer flow during the simulation process, all parts of the wall were added to the prism mesh in this study, and the grid was set to 5 layers. Before the particle quantity sensitivity analysis, we also completed a mesh independence study. The nodes' quantities were, respectively, from 1.3 million to 6.3 million. The three-dimensional computational domain was discretized to an unstructured grid using the ICEM CFD meshing tool. As shown in Figure 3, with the number of nodes at more than 4.2 million, the result of the steam quality at the orifice outlet changed within 3% from 4.2 million nodes to 6.3 million nodes. The changes were calculated by the function $C_{change} = (SQ_2 - SQ_1)/SQ_1$, where SQ represents the steam quality with different mesh quantities. Thus, the study simulation of different conditions used the same order of magnitude as for node quantities over 4 million.
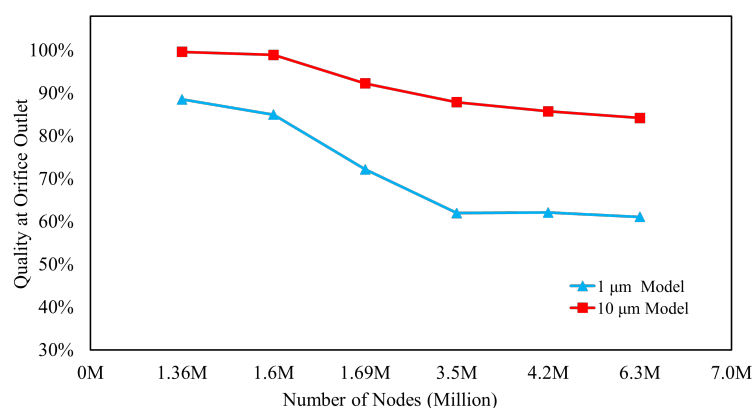
Figure 3. Results of mesh independence.

Generally, this study was based on a well-known moisture separator model. Most work was completed in the ANSYS platform. The preprocessing was based on the ANSYS ICEM CFD. The solving process applied was ANSYS CFX, which is known as a fully implicit coupled solver. As mentioned before, the turbulence model applied was the SST $k - \omega$ model, and the multiphase model was based on the particle transport theory. The discretization schemes in this study were chosen using the high-resolution method in CFX. The linear equations were solved using an algebraic multigrid method (AMG). Additionally, postprocessing was applied via ANSYS CFD-post.

2.3. Problem Description

To study the influence of different structures of the swirl vane separator, three different geometries—with different vane bending angles, different vane quantities, and different vane locations—were used. Figures 4–6 show the schematics of these different structures, respectively.

Figure 4 shows the vane bending angle α as the angle between the curved line of the swirl vane and the horizontal line. Four angle cases, namely, 20°, 30°, 40°, and 50°, were chosen. Figure 5 shows the variation in swirl vane quantities from 3 to 6. Figure 6 shows the different vane locations, where Y denotes the distance from the outline of the vane bottom to the original vane bottom outline. The reference model origin point was defined as the distance between the orifice outlet plane and the swirl start plane, which was equal to 1400 mm. The case with a bending angle of 30°, 4 vanes, and Y = 0 was taken as the reference model.

The physical parameters and boundary conditions used in this study are shown in Table 1. The real operation conditions of the power plant were applied as the simulation conditions. The steam inlet mass flow rate and pressure were fixed as 30 kg/s and 6.9 MPa. The droplet particle size ranged from 1 to 50 μm for all cases to investigate the influence on particle size. Forty-five cases were analyzed in this study and were divided into 4 groups. The pressure drop results were classified into 3 groups to visualize the effect of different

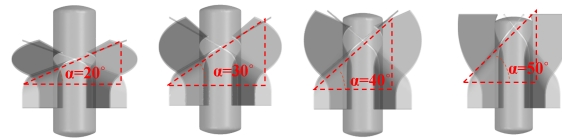geometries. The classification details are shown in Table 2. Related discussions are provided

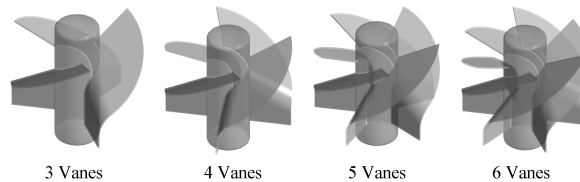**Figure 4.** Schematic of different vane bending angles.

3 Vanes   4 Vanes   5 Vanes   6 Vanes

Figure 5. Schematic of different swirl vane quantities.
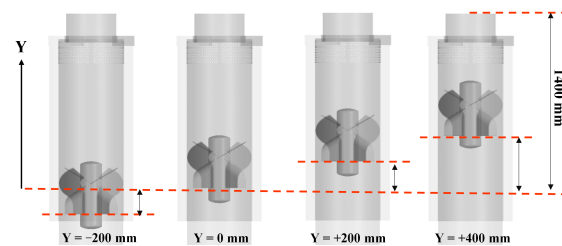

Y = −200 mm   Y = 0 mm   Y = +200 mm   Y = +400 mm

Figure 6. Schematic of the different swirl vane locations from the origin.

Table 1. Summary of input parameters.

Properties	Values	Units
Inlet steam mass flow rate	30	kg/s
Inlet particle mass flow rate	90	kg/s
Inlet pressure	6.9	MPa
Inlet temperature	300	°C
Outlet pressure	0	MPa
Bending angle of swirl vane	20, 30, 40, 50	deg
Swirl vane quantity	3, 4, 5, 6	-
Swirl vane location	−200, 0, 200, 400	mm
Particle size	0.01, 0.1, 1, 10, 30, 50	μm
Injected particle quality	25	%

The information about the droplet particle size distribution could be obtained from relevant references [37–40], and the following conclusions could be made. When the number of droplet particles was large enough, the droplet size followed the law of a normal distribution, which is a continuous probability distribution of a random variable whose logarithm is normally distributed. Through this theory, we could further analyze the steam quality difference in this paper. The mathematical relationship between the steam quality result under a specific particle size and the real steam quality result could be determined. We provide the expression of the droplet size normal distribution as follows:

$$f(D) = A \frac{1}{D\sigma\sqrt{2x}} exp - \left(\frac{(\ln D - \ln D_{av})^2}{2\sigma^2} \right) \tag{10}$$

where D represents the diameter of the droplet, D_{av} represents the average droplet size in this paper, and σ represents the standard deviation of the droplet size. The average droplet size was set to be 138 μm, the standard variance $\sigma = 0.5514$, and the amplitude coefficient $A = 530$ [40]. The droplet particle size normal distribution is shown in Figure 7.
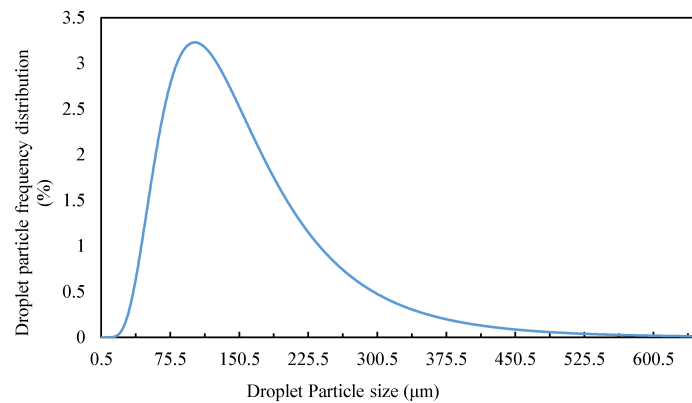

Figure 7. Droplet particle size normal distribution.

After integrating the equation, the cumulative distribution function could be obtained. After multiplying and summing the result of the numerical solution in this paper and the result of the distribution function, we obtained the theoretical real steam quality at the outlet of the moisture separator. The function was as follows:

$$Q_{total} = \sum_0^{Maxsize}(Q_n F_n) \tag{11}$$

Q_{total} represents the steam quality after the separator, Q_n represents the simulated results of the steam quality after the steam separator at a specific droplet size n, and F represents the percentage of the corresponding droplet size n obtained by the distribution function. Through this formula, we could calculate the real outlet steam quality of moisture separators of different structures.

Table 2. Classification groups of the pressure drop results.

	Case 1	**Case 2**	**Case 3**	**Case 4**
Bending angle	20 deg	30 deg	40 deg	50 deg
Vane quantity	3	4	5	6
Vane location	−200 mm	0	200 mm	400 mm

3. Results and Discussion

In this section, several flow fields are presented to briefly describe the separator flow. These results are based on the reference model with a bending angle of 30°, four swirl vanes, and a reference swirl vane location.

Figure 8 shows the pressure and velocity distribution of the reference model. The pressure decreased when the mixture flowed through swirl vanes. The velocity magnitude distribution had a different trend when the mixture flowed through the swirl vanes. The maximum velocity could be found at the bending point of the swirl vanes. The velocity magnitude of moisture was at a relatively low level compared to the location after the swirl vanes. On the contrary, when moisture flowed through the swirl vane, the velocity was significantly rotated. Finally, the fluid entered the downcomer through the holes in the riser, and the remaining part flowed into the tangent nozzle outlet and the orifice

outlet. The reason for the sudden change in velocity and pressure was that the flow section area shrunk at the swirl vane. Similar results were found by He et al. [41] and Fang et al. [24]. The distribution of velocity in the separator changed sharply near the swirl vane. The corresponding visualizations can be seen in Figure 9 for different locations along the Y axis. Y = −150 mm and Y = 1400 mm represent the moisture separator's bottom and top, respectively. The figure at −150 mm shows that the mixture flow had no swirl before the swirl vane. As the flow went up to 200 mm, a strong swirling flow was generated. At 1000 mm, it was clear that part of the mixture would flow out of the riser holes. Tian et al. [21] found a similar distribution in sectional views. The above shows that the particle separated from the mixture process. Because of the swirl generated, several particles moved toward the wall and were captured by the wall. Several particles flowed out from the riser holes.
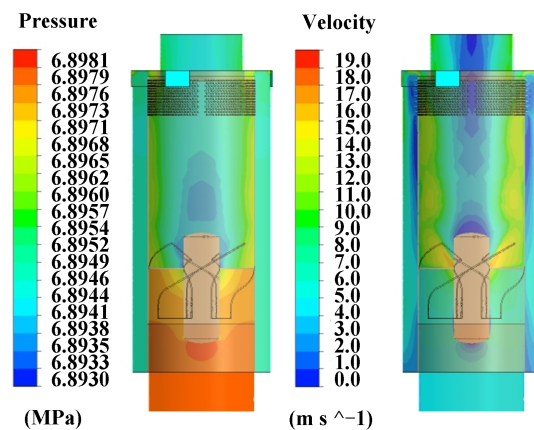
Figure 8. Pressure and velocity magnitude distribution of the reference model.
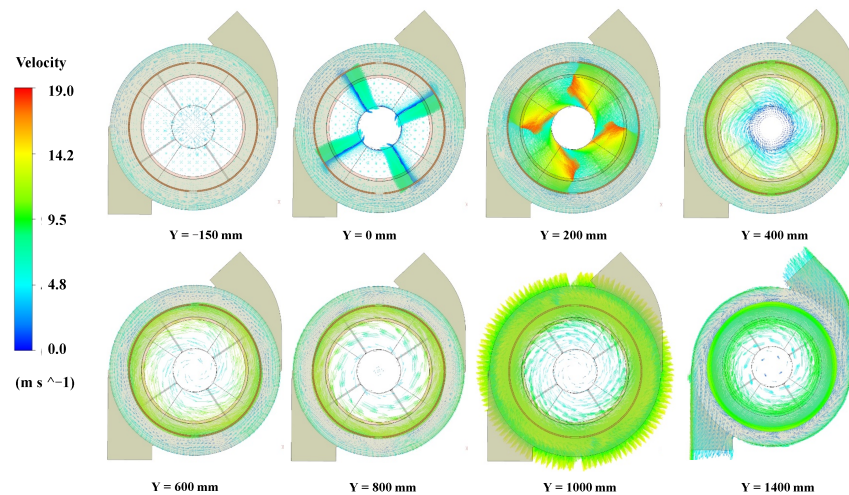

Figure 9. Velocity vector contours from Y = −150 mm to Y = 1400 mm in the reference model.

3.1. Droplet Separation Process

In this section, the effect of different structures on the droplets captured on the separator wall is considered . The results are summarized based on the reference model. Using the particle tracking method to simulate the process provided a simple way of capturing the water droplets' motion features during the process of the steam flow [31]. It allowed us to understand the correlation principle of the particles being captured by the wall in the separator.

Firstly, in Figure 10, the streamline and velocity isosurface of the moisture flow are shown. It is obvious that the moisture obtained a swirl component during the process of

passing through the swirl vanes. This caused the moisture to flow in the vertical direction with a tangential velocity. The droplet particles in the mixture fluid were collected by the riser wall when they encountered it. For the mixture, the density gap between the vapor and droplet particles were utilized for this process. As the density of the droplets was greater than that of the steam, the particles were subjected to a greater centrifugal force. Based on this principle, the swirl velocity in the separator needed to be increased if the droplets were to easily migrate to the wall.

The results related to the particle size are summarized in the following sections. When the droplet particle diameter increased, the mass of the droplets was continuously increased. This led to an increase in the centrifugal force of the droplet particles. The particles moved in the direction of the center of the cut surface and were captured by the wall. All three structures made use of this centrifugal force. As in the other two sections, the results show that the change in the swirl vane angle had the highest influence on particle capture.

In contrast, Fang et al. [23] concluded that, when the particle diameter exceeded 102 μm, all droplet particles were separated from the steam, and Matsubayashi et al. [8] illustrated that the critical particle size was 25 μm. These different results are due to the different inlet steam velocity in these investigations. Our results showed a critical particle size of around 50 μm because the inlet velocity was higher than in previous studies. It is understood that different researchers have different critical particle sizes due to the particle collection rate. The results came from different kinds of geometries and various definition conditions in the simulations.
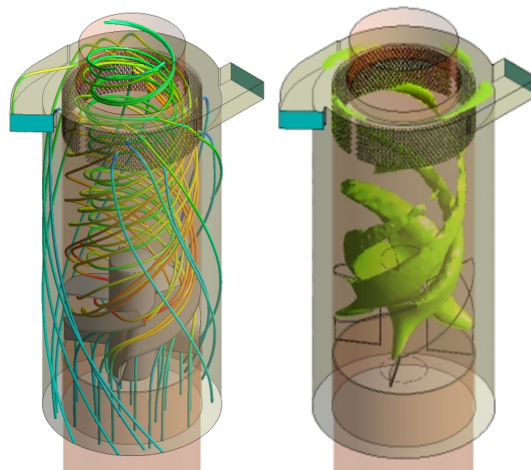

Figure 10. The streamline and velocity isosurface of the moisture flow.

3.2. Effect of the Vane Bending Angle

Figure 11 shows the rate of particles collected on the wall with changing vane angles and droplet sizes. The vertical axis is the ratio of water droplets removed by wall collisions. As the droplet size increased, the rate of particles collected on the wall increased. A vane bending angle from 20° to 50° maintained a constant collection rate if the droplet size was less than 1μm. A vane angle of 20° had the highest particle collection rate, and a vane bending angle of 50° had the lowest collection rate, even at 50 μm. Moreover, the critical particle size, which is a collection rate on the wall of 100% at a certain particle size, was 10~30 μm in the 20° model, 30~50 μm in the 30° model, and over 50 μm in the 40° model.

Figure 12 shows the pressure drop between the inlet and orifice outlet for various bending angles. With the bending angle changing from 20° to 50°, the pressure dropped by 6444, 3035, 1579, and 820.5 Pa, respectively, which implied that the pressure of the separator decreased gradually as the bending angle increased. As the vane angle decreased by 10°, the pressure drop increased to nearly twice that of the higher angle. The figure shows that a vane angle of 50° had the lowest pressure drop. Because the swirl vanes were fixed in the moisture separator, the flow section areas decreased in the axis direction. This caused

the local friction to increase, meaning that the pressure drop increased at the same time. It can be understood from the conservation of energy that the reduction of the pressure term would result in an increase in the velocity term and the internal energy.

The steam that passes through the orifice outlet directly passes through the secondary moisture separator and then flows to the turbine. As the steam quality in a moisture separator outlet should be at least 80% [34], the steam that flows out of the primary moisture separator should maintain a high quality to ensure the stability and efficiency of the turbine. The steam quality can be calculated by using Equation (12).

$$\chi = \frac{\dot{m}_{steam}}{\dot{m}_{steam} + \dot{m}_{waterdroplet}} \tag{12}$$

Figure 13 shows the steam quality at the orifice outlet for various swirl vane bending angles. The size of the droplet had no effect if the bending angle was 20°. The steam quality in the direction of the orifice outlet was 100%, which implied that all water droplets were separated from the steam. When the vane angle was 30°, the steam quality began at 62% at a particle size of 1 μm and was 100% at 50 μm. For a vane angle of 40°, the steam quality began at 32.3% at a particle size of 1 μm and reached 100% at over 50 μm. The geometry with a vane angle of 50° yielded the lowest efficiency in terms of steam quality; even for a particle size of 50 μm, the orifice steam quality was only 40%. There were two reasons for this. Firstly, reducing the bending angle increased the resistance. This increased the local velocity. Secondly, the increase in particle diameter directly caused the mass of the droplet particles to increase. From the centrifugal force formula, the centrifugal force increased as the speed increased, and the mass increased. Fang et al. [2] illustrated a separation efficiency change from 98.2% to 99.4% during a steam velocity increase from 2.5 m/s to 6 m/s. As our inlet velocity was greater than that, an orifice outlet steam quality of 100% was acceptable.
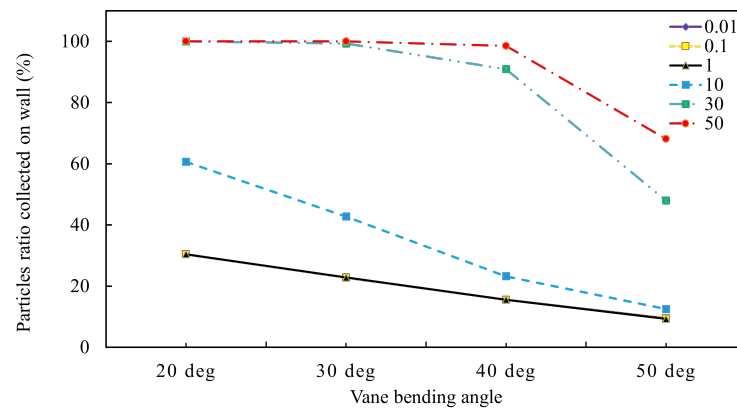

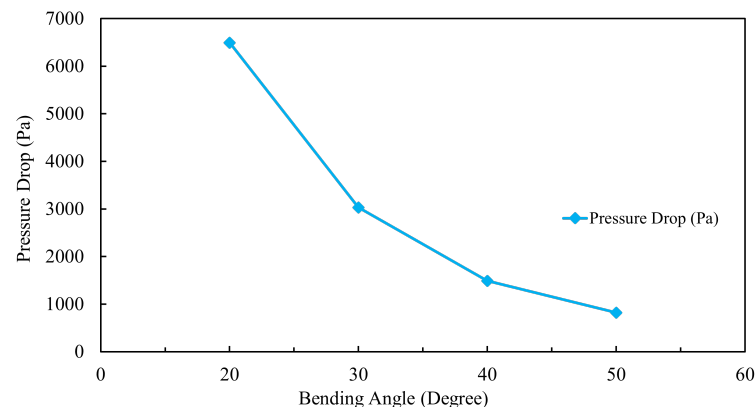**Figure 11.** Effect of vane bending angles with different particle sizes.

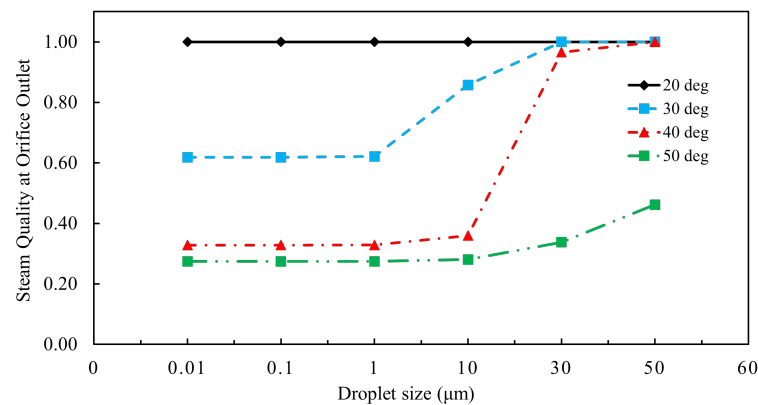**Figure 12.** Pressure drop between the inlet and orifice outlet for various bending angles.

Figure 13. Steam quality at the orifice outlet for various droplet sizes and vane bending angles.

3.3. Effect of Vane Quantity

The probability of trapping droplet particles on the wall increased as the swirl vane quantities increased, as shown in Figure 14. The vane quantity had little effect on particle collection. The particles were all captured by the wall when the diameter of the particles reached 30 μm, implying that all particles were separated from the steam if the diameter exceeded 30 μm.

Figure 15 shows the pressure drop between the inlet and outlet pressure of the moisture separator for various vane quantities. The pressure drop increased as the swirl vane quantity increased, implying that the resistance along the inside of the separator increased significantly. However, compared with the previous changing bending angle, the result was not as obvious. Thus, the flow section areas reduced more slowly as swirl vane quantities changed.

Figure 16 shows the steam quality at the orifice outlet for various swirl vane quantities. For six vanes, the steam quality in the direction of the orifice outlet exceeded 95%, which means that almost all water droplets were separated from the steam. For 3–6 vanes, the steam quality started from 56%, 62%, 74%, and 93%, respectively. Thus, the steam quality increased as the vane quantity increased. Similar results were found when more swirl vanes were fixed in the separator. As a result, the local resistance increased, which immediately led to a significant increase in speed. The droplet particles were subjected to more centrifugal force in this process, which was why the steam quality increased.
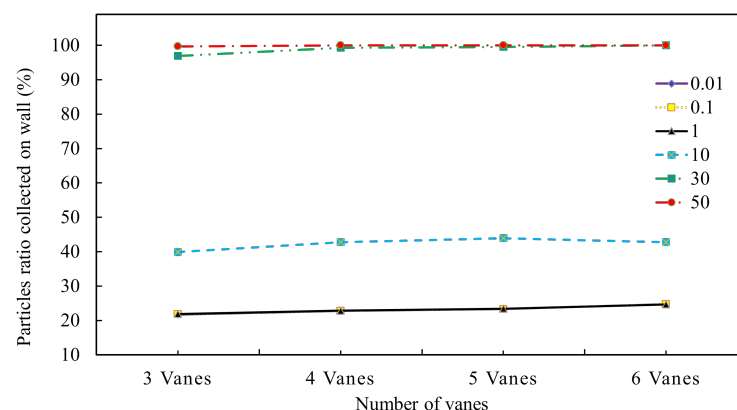

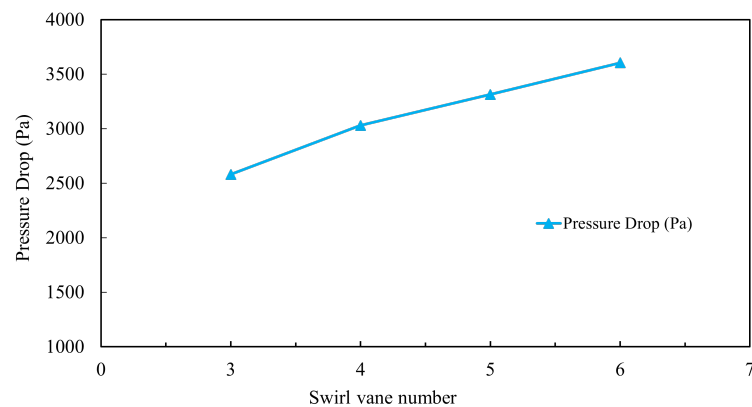**Figure 14.** Effect of vane quantities with different particle sizes.

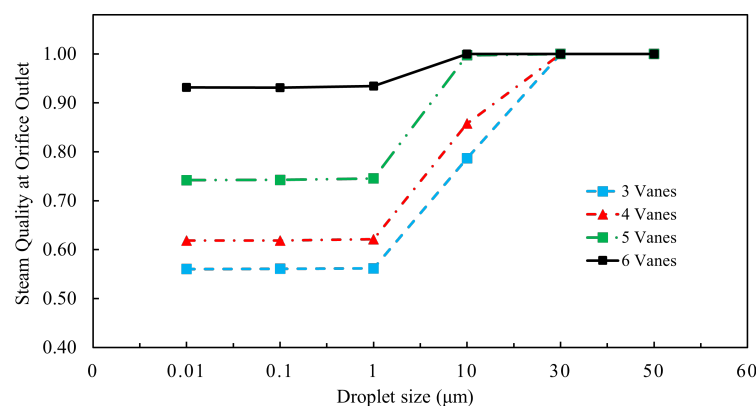**Figure 15.** Pressure drop between the inlet and outlet for various vane quantities.

Figure 16. Steam quality at the orifice outlet for various droplet sizes and vane quantities.

3.4. Effect of Vane Location

Figure 17 shows the simulation results of the particle collection rate at different vane locations and for different droplet sizes. The figure shows that the particle collection rate increased as the droplet size increased. However, the particle collection rate changes were not very significant at different vane positions. Nevertheless, raising the vane location increased the particle collection rate. This implied that when the location of the swirl vane was close to the orifice outlet, a higher particle collection rate was found.

Figure 18 shows the pressure drop between the inlet and outlet pressure of the moisture separator at various vane locations. There was no significant pressure drop at various swirl vane locations, except for the location near the orifice outlet, as shown in the figure. Even this pressure increase near the orifice added only about 100 Pa. This pressure drop seems reasonable when compared with the case where the vane bending angle and the swirl vane quantity changed. Changing the swirl vane location did not increase the local resistance.

Figure 19 shows the steam quality at the orifice outlet at various vane locations. The steam quality changed from 37% to 91%, respectively, when the vane location changed from −200 to 400 mm. The greater the distance between the swirl vane and the orifice outlet plane, the higher the steam quality at the outlet. In addition, when the particle size was larger than 30 microns, the quality of the steam became 100%, implying that all droplets were being separated from the steam. This result is consistent with previous results shown in Figures 15 and 17. The reason for this is mainly that the droplet particles were subjected to centrifugal force, and it took a certain amount of time to move from the inside of the separator to the riser wall. When the position of the swirl vanes was raised, the droplet particles were not captured by the wall collision, and they flowed directly out of the moisture separator. This caused the increase in the position of the rotor, which reduced the steam quality.
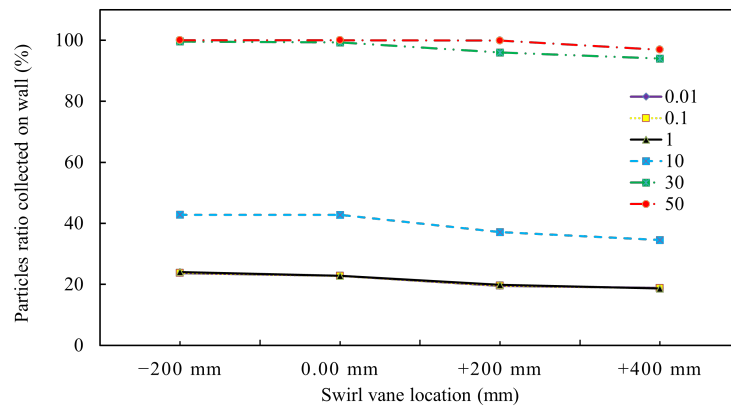
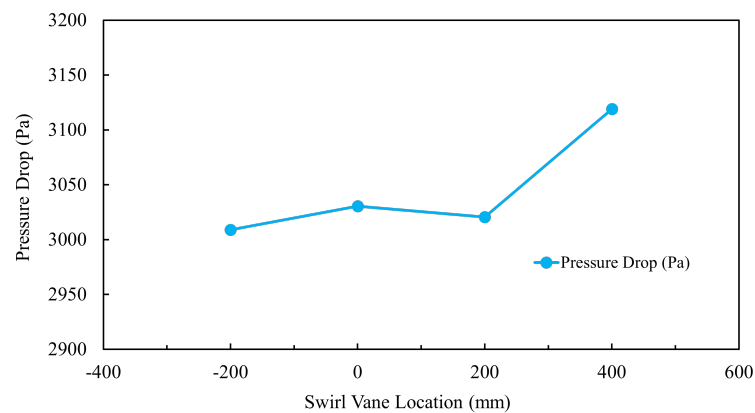**Figure 17.** Effect of vane location with different particle sizes.

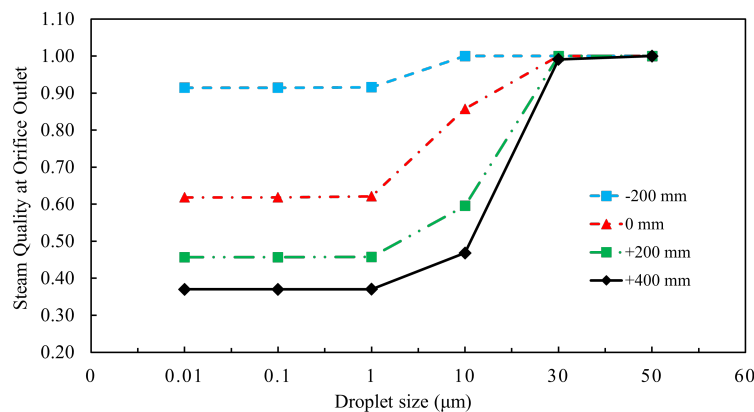**Figure 18.** Pressure drop between the inlet and outlet at various vane locations.

Figure 19. Steam quality at the orifice outlet for various droplet sizes and vane locations.

Figure 20 shows the classification and comparison of the pressure drop results for the three different structures, respectively. In Figure 13, the swirl vane bending angle had the highest impact on the pressure drop, whereas the swirl vane location changes had the weakest effect. The changes in the drag factor of various structures increased the local resistance. The separator design specifications of Westinghouse indicate that the pressure drop of the swirl vane separator should be less than 2.8 psi (19.3 kPa) [42]. Thus, although decreasing the angle of the swirl vanes caused a substantial pressure drop, the result met the requirements of the design specification (in this study, a maximum of 7 kPa).

From the above results, changing the bending angle of the swirl vane had the greatest effect on steam quality. When the bending angle of the vane was 50°, the steam quality of the orifice outlet only reached 46%. In the process of changing the number of swirl vanes and their positions, the steam quality could be maximized when the droplet size was

greater than 30μm. In these three structures, the purpose of changing the bending angle, quantities, and locations was to increase the swirling velocity of the moisture, subjecting the particles to more centrifugal force. While changing the position of the swirl vanes from 400 to −200 mm, the particles took more time moving from the inside to the riser surface. All three of the above methods could effectively improve the steam quality at the orifice outlet.
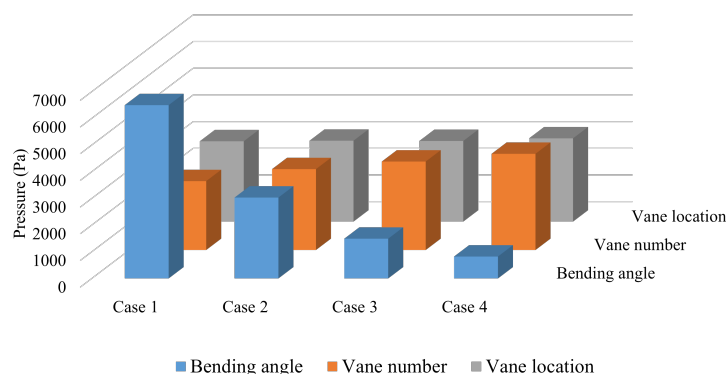

Figure 20. Comparison of different structure effects on pressure drop.

In Figure 13, the steam qualities with a bending angle of 30° were 0.62, 0.62, 0.62, 0.86, 1, and 1, respectively, with different droplet particle sizes. The total steam quality was 99.99% based on Equation (11). Applying a similar method to other cases, the total steam quality was 100%, 99.99%, 99.54%, and 44.49% as the bending angle changed from 20° to 50°. In addition, the total steam quality values with changing swirl vane quantities and locations were all over 99%. This showed that changes in the droplet particle size within 50 microns did not have a significant impact on the total steam quality. The reason for this can be attributed to the fact that most of the droplet particles are larger than 50 microns in size [43].

4. Conclusions

The characteristics of a PWR's primary moisture separator were analyzed in this study. A study was conducted on three parameters affecting the quality of the steam: swirl vane angle, swirl vane quantity, and swirl vane location. Different water droplet sizes from 0.01 to 50 μm were also considered. The results of a pressure drop between the inlet to the outlet, the steam quality at the orifice outlet, and the particle collection rate on the wall of the moisture separator were analyzed. The results were as follows:

Firstly, the steam quality increased as the bending angle decreased. However, the pressure drop between the inlet to the outlet increased during this process. When the vane angle decreased by 10°, the pressure drop increased nearly twice as much. This showed that changing the vane bending angle had the greatest influence on the pressure drop.

Secondly, when the swirl vane quantity increased, both the pressure drop and steam quality increased. In addition, increasing the distance between the swirl vane location and the reference line increased the steam quality significantly but involved a relatively small pressure drop. The simulation results thus showed that a new moisture separator design that improved steam quality at the orifice outlet involved a significant pressure drop. However, even a pressure drop in a model with a bending angle of 20° could provide results that met the Westinghouse design specifications.

Finally, these three moisture separator structure changes had an effect only when the particle size was below 50 μm, because all particles were collected on the wall if the particle size was over 50 μm.

Author Contributions: H.Z.: conceptualization, methodology, investigation, visualization, and writing—original draft; J.H.J.: investigation, writing—review and editing; D.I.Y.: methodology, writing—review and editing; Y.W.L.: conceptualization, supervision, project administration, funding

References

1. Exxonmobil. 2018 Outlook for Energy: A View to 2040. Report, 2018. Available online: https://www.aop.es/wp-content/uploads/2019/05/2018-Outlook-for-Energy-Exxon.pdf (accessed on 1 July 2019).
2. Fang, D.; Li, L.; Li, J.; Wang, M.; Yu, H.; Zhang, J.; Qiu, S.; Tian, W.; Su, G.H. Full-scale numerical study on the thermal-hydraulic characteristics of steam-water separation system in an advanced PWR UTSG. Part two: Droplets separation process. *Prog. Nucl. Energy* **2020**, *118*, 103139. [CrossRef]
3. Gupta, A.K.; Lilley, D.G.; Syred, N. *Swirl Flows*; Abacus Press: Tunbridge Wells, UK, 1984; 488p.
4. Kataoka, H.; Shinkai, Y.; Tomiyama, A. Effects of Swirler Shape on Two-Phase Swirling Flow in a Steam Separator. *J. Power Energy Syst.* **2009**, *3*, 347–355. [CrossRef]
5. Qu, J.; Yan, T.; Sun, X.; Li, Z.; Li, W. Decaying Swirl Flow and Particle Behavior through the Hole Cleaning Device for Horizontal Drilling of Fossil Fuel. *Energies* **2019**, *12*, 336. [CrossRef]
6. Najafi, A.F.; Mousavian, S.M.; Amini, K. Numerical investigations on swirl intensity decay rate for turbulent swirling flow in a fixed pipe. *Int. J. Mech. Sci.* **2011**, *53*, 801–811. [CrossRef]
7. Saqr, K.M.; Wahid, M.A. Effects of swirl intensity on heat transfer and entropy generation in turbulent decaying swirl flow. *Appl. Therm. Eng.* **2014**, *70*, 486–493. [CrossRef]
8. Liu, L.; Bai, B. A mechanistic model for the prediction of swirling annular flow pattern transition. *Chem. Eng. Sci.* **2019**, *199*, 405–416. [CrossRef]
9. Liu, L.; Bai, B. Scaling laws for gas-liquid flow in swirl vane separators. *Nucl. Eng. Des.* **2016**, *298*, 229–239. [CrossRef]
10. Matsubayashi, T.; Katono, K.; Hayashi, K.; Tomiyama, A. Effects of swirler shape on swirling annular flow in a gas-liquid separator. *Nucl. Eng. Des.* **2012**, *249*, 63–70. [CrossRef]
11. Funahashi, H.; Hayashi, K.; Hosokawa, S.; Tomiyama, A. Study on two-phase swirling flows in a gas-liquid separator with three pick-off rings. *Nucl. Eng. Des.* **2016**, *308*, 205–213. [CrossRef]
12. Funahashi, H.; Hayashi, K.; Hosokawa, S.; Tomiyama, A. Improvement of separator performance with modified pick-off ring and swirler. *Nucl. Eng. Des.* **2017**, *322*, 360–367. [CrossRef]
13. Nishida, K.; Mizutani, T.; Suzuta, T.; Kondo, Y.; Hirao, Y. Development of Moisture Separator With High Performance of Steam Generator. In Proceedings of the 12th International Conference on Nuclear Engineering, Arlington, VI, USA, 25–29 April 2004; Volume 3, pp. 545–550. [CrossRef]
14. Xiong, Z.; Lu, M.; Li, Y.; Gu, H.; Cheng, X. Effects of the slots on the performance of swirl-vane separator. *Nucl. Eng. Des.* **2013**, *265*, 13–18. [CrossRef]
15. Kataoka, H.; Tomiyama, A.; Hosokawa, S.; Sou, A.; Chaki, M. Two-Phase Swirling Flow in a Gas-Liquid Separator. *J. Power Energy Syst.* **2008**, *2*, 1120–1131. [CrossRef]
16. Funahashi, H.; Vierow Kirkland, K.; Hayashi, K.; Hosokawa, S.; Tomiyama, A. Interfacial and wall friction factors of swirling annular flow in a vertical pipe. *Nucl. Eng. Des.* **2018**, *330*, 97–105. [CrossRef]
17. Versteeg, H.K.; Malalasekera, W. *An Introduction to Computational Fluid Dynamics: The Finite Volume Method*; Pearson Education: London, UK, 2007.
18. Tamrina, K.F.; Sheikhb, N.A.; Rahmatullaha, B.; Malim, T. Numerical Analysis of Swirl Intensity in Turbulent Swirling Pipe Flows. *J. Teknol.* **2015**, *76*, 362–372.
19. Zhang, H.; Liu, Q.; Qin, B.; Bo, H.; Chen, F. Study on working mechanism of AP1000 moisture separator by numerical modeling. *Ann. Nucl. Energy* **2016**, *92*, 345–354. [CrossRef]
20. Zhang, H.; Bo, H.; Chen, F. Numerical Simulation of Separation Efficiency and Pressure Drop of AP1000 Swirl-Vane Moisture Separator. *Nucl. Power Eng.* **2015**, *36*, 75–79. [CrossRef]
21. Tian, Z.; Yang, L. Numerical Investigation on a New Type of Two-Stage Steam Separator in Pressurized Water Reactors. *Energy Procedia* **2017**, *142*, 3962–3967. [CrossRef]
22. Kataoka, H.; Shinkai, Y.; Tomiyama, A. Pressure Drop in Two-Phase Swirling Flow in a Steam Separator. *J. Power Energy Syst.* **2009**, *3*, 382–392. [CrossRef]
23. Song, J.; Guo, H.; Yao, Q.; Jiang, R. The modeling and simulation analysis on steam generator working process. *Chin. J. Nucl. Sci. Eng.* **2007**, *27*, 27–31.

24. Fang, D.; Wang, M.; Duan, Y.; Li, J.; Qiu, G.; Tian, W.; Zuo, C.; Su, G.H.; Qiu, S. Full-scale numerical study on the flow characteristics and mal-distribution phenomena in SG steam-water separation system of an advanced PWR. *Prog. Nucl. Energy* **2020**, *118*, 103075. [CrossRef]

25. Saito, Y.; Aoyama, G.; Souma, H.; Nakao, T.; Sumida, I. Analysis of Droplet Behavior in BWR Separator. *J. Nucl. Sci. Technol.* **1994**, *31*, 349–351. [CrossRef]

26. Katono, K.; Ishida, N.; Sumikawa, T.; Yasuda, K. Air-water downscaled experiments and three-dimensional two-phase flow simulations of improved steam separator for boiling water reactor. *Nucl. Eng. Des.* **2014**, *278*, 465–471. [CrossRef]

27. Xiong, Z.; Lu, M.; Wang, M.; Gu, H.; Cheng, X. Study on flow pattern and separation performance of air-water swirl-vane separator. *Ann. Nucl. Energy* **2014**, *63*, 138–145. [CrossRef]

28. Rocha, A.D.; Bannwart, A.C.; Ganzarolli, M.M. Numerical and experimental study of an axially induced swirling pipe flow. *Int. J. Heat Fluid Flow* **2015**, *53*, 81–90. [CrossRef]

29. Fang, J.; Cambareri, J.J.; Brown, C.S.; Feng, J.; Gouws, A.; Li, M.; Bolotnov, I.A. Direct numerical simulation of reactor two-phase flows enabled by high-performance computing. *Nucl. Eng. Des.* **2018**, *330*, 409–419. [CrossRef]

30. ANSYS, Inc. *ANSYS CFX-Solver Theory Guide*; Release 16.2; ANSYS, Inc.: Canonsburg, PA, USA, 2015.

31. ANSYS, Inc. *ANSYS CFX-Solver Modeling Guide*; Release 16.2; ANSYS, Inc.: Canonsburg, PA, USA, 2015.

32. Fang, J.; Cambareri, J.J.; Li, M.; Saini, N.; Bolotnov, I.A. Interface-resolved simulations of reactor flows. *Nucl. Technol.* **2020**, *206*, 133–149. [CrossRef]

33. Afrasiabi, M.; Roethlin, M.; Wegener, K. Thermal simulation in multiphase incompressible flows using coupled meshfree and particle level set methods. *Comput. Methods Appl. Mech. Eng.* **2018**, *336*, 667–694. [CrossRef]

34. Kolev, N.I. *Multiphase Flow Dynamics 5: Nuclear Thermal Hydraulics*; Springer Science & Business Media: Berlin, Germany, 2007; Volume 5.

35. Blazek, J. *Computational Fluid Dynamics: Principles and Applications*; Elsevier Science: Amsterdam, The Netherlands, 2015.

36. Masatsuka, K. *I Do Like CFD*, 2nd ed.; Lulu Press, Inc.: Morrisville, NC, USA, 2013; Volume 1.

37. ZHOU, X.; Gao, S. Confidence intervals for the log-normal mean. *Stat. Med.* **1997**, *16*, 783–790. [CrossRef]

38. Katolicky, J.; Jicha, M.; Mares, R. Droplets deposition in steam piping connecting steam generator and steam turbine in nuclear plant. *Nucl. Eng. Des.* **2007**, *237*, 1534–1549. [CrossRef]

39. Olsson, U. Confidence intervals for the mean of a log-normal distribution. *J. Stat. Educ.* **2005**, *13*, 1–9. [CrossRef]

40. Jin, Y.; Miller, D.J.; Qiao, S.; Rau, A.; Kim, S.; Cheung, F.B.; Bajorek, S.M.; Tien, K.; Hoxie, C.L. Uncertainty analysis on droplet size measurement in dispersed flow film boiling regime during reflood using image processing technique. *Nucl. Eng. Des.* **2018**, *326*, 202–219. [CrossRef]

41. He, X.; Liu, Q.; Zhang, H.; Kui, M.Q.; Tan, X.H.; Li, X.P. Numerical investigation of the performance of moisture separators based on two-way coupling model by Lagrangian-Eulerian methodology. *Ann. Nucl. Energy* **2019**, *124*, 407–417. [CrossRef]

42. Commission, U.S.N.R. Delta 53 RSG Thermal Hydraulic Design Analysis Report for UCN1&2 RSG, 2021. Available online: https://www.nrc.gov/docs/ (accessed on 10 February 2021).

43. Jun-Ho, J.; Hong-Wu, Z.; Young-Kyu, P.; Yeon-Won, L. Numerical Analysis of Swirl-Vane Separator Using Particle Tracking Method. *J. Power Syst. Eng.* **2020**, *24*, 30–36. [CrossRef]